Available online at www.sciencedirect.com
ScienceDirect
Journal of Power Sources 169 (2007) 296–314
JOURNAL OF POWER SOURCES
www.elsevier.com/locate/jpowsour

Innovative gas diffusion layers and their water removal characteristics in PEM fuel cell cathode

Kui Jiao, Biao Zhou *

Department of Mechanical, Automotive & Materials Engineering, University of Windsor, Ont., Canada N9B 3P4

Received 14 February 2007; received in revised form 15 March 2007; accepted 15 March 2007
Available online 24 March 2007

Abstract

Liquid water transport is one of the key challenges regarding the water management in a proton exchange membrane (PEM) fuel cell. Conventional gas diffusion layers (GDLs) do not allow a well-organized liquid water flow from catalyst layer to gas flow channels. In this paper, three innovative GDLs with different micro-flow channels were proposed to solve liquid water flooding problems that conventional GDLs have. This paper also presents numerical investigations of air–water flow across the proposed innovative GDLs together with a serpentine gas flow channel on PEM fuel cell cathode by use of a commercial computational fluid dynamics (CFD) software package FLUENT. The results showed that different designs of GDLs will affect the liquid water flow patterns significantly, thus influencing the performance of PEM fuel cells. The detailed flow patterns of liquid water were shown. Several gas flow problems for the proposed different kinds of innovative GDLs were observed, and some useful suggestions were given through investigating the flow patterns inside the proposed GDLs.

Keywords: Water management; Air–water flow pattern; Gas diffusion layer (GDL); CFD

1. Introduction

Low operating temperature and zero/low emissions have made proton exchange membrane (PEM) fuel cells become the most promising power source of the future [1]. However, to achieve commercialization, the performance of PEM fuel cells needs to be improved by proper engineering design and optimization. Due to the special chemical structure of the PEM, the membrane must be well hydrated to ensure that a sufficient amount of hydrogen ions could cross. On the other hand, due to the low operating temperature of PEM fuel cells (30–100 °C) [1], excessive humidification could result in water vapour condensation that could subsequently block the gas flow channels resulting in a lower air flow rate on the cathode side, thus decreasing fuel cell performance. Water content is also an important factor that affects the ohmic resistance in the membrane [2]. Therefore, keeping an appropriate amount of water content in the fuel cell to avoid both membrane dehydration and water vapour condensation has been a critical issue in improving fuel cell performance. In reality, however, it is almost impossible to manage water on both the anode and cathode sides without dehydration and condensation; this is simply because water vapour condensation in the gas flow channels of practical fuel cell applications is unavoidable [2]. Therefore, water management, to which many engineers and scientists have recently paid particular attention, has been a critical challenge for a high-performance fuel cell design and optimization. A comprehensive review of water management in fuel cells was also made by Wang [3] to address this important issue.

In the last decade, water management related studies were performed numerically and experimentally for different purposes and in several ways. A CFD modeling of PEM fuel cells which simultaneously considered the electrochemical kinetics, current distributions, hydrodynamics, and multi-component transport was conducted by Um et al. [4]. A three-dimensional (3D) numerical simulation of a straight gas flow channel in a PEM fuel cell was performed by Dutta et al. [5] using a commercial CFD software FLUENT. Hontanon et al. [6] also employed FLUENT to implement their 3D, stationary gas flow model. A study exploring the steady-state gas transport phenomena in micro-scale parallel flow channels was conducted by Cha et al. [7] in which oxygen concentration along a single gas flow chan-

* Corresponding author. Tel.: +1 519 253 3000x2630; fax: +1 519 973 7007.
E-mail address: bzhou@uwindsor.ca (B. Zhou).

0378-7753/$ – see front matter © 2007 Elsevier B.V. All rights reserved.
doi:10.1016/j.jpowsour.2007.03.042

nel and other flow patterns that may affect fuel cell performance were discussed. Similarly, gas concentration of a steady-state flow along fuel cell flow channels was obtained numerically by Kulikovsky [8]. However, in all the studies mentioned above, the effects of liquid water were neglected. Yi et al. [2] pointed out that water vapour condensation was inevitable on both the anode and cathode sides of a PEM fuel cell, and they discussed a liquid water removal technique that used a water transport plate to lead excess liquid water to the coolant flow channels by a pressure difference. Wang el al. [9] conducted a two-phase model on PEM fuel cell cathode to address the liquid water concentrations. You and Liu [10] also considered liquid water concentration in a straight channel on the cathode side. Both the references [9,10] showed the importance for considering liquid water in numerical modeling of PEM fuel cells. In recent years, more two phase models have been published [11–13], these simulations predicted water flooding inside PEM fuel cells, and the liquid water effects on PEM fuel cell performances. Large-scale simulations for complex flow field were also performed with experimental validations [14–17], these simulations provided more realistic results rather than considering one single cell.

By far, to the authors' knowledge, most of the two phase numerical models have not considered the interface tracking between liquid water and gas. The detailed behaviours of liquid water transport inside the PEM fuel cells were rarely discussed except for the present authors' previous study [18], which only dealt with part of serpentine channels—the single U-shaped channel. Recently, the authors also conducted two more studies that dealt with liquid water in serpentine and straight parallel fuel cell stacks [19,20].

On the cathode side of fuel cells, most of the water, which is mainly produced by the electrochemical reaction, diffuses through the gas diffusion layer (GDL) to the gas flow channels. Therefore, liquid water flow across these porous mediums to the gas flow channels, and formation of water droplets during this process are both unavoidable and important for practical operations of PEM fuel cells. As the authors reviewed, experimental studies to probe detailed liquid water transport from the GDL into the gas flow channels have been performed by Yang el al. [21] and Zhang et al. [22]. In these studies, the observations of liquid water distributions on the GDL surfaces were made in a transparent PEM fuel cell, and liquid water droplet formation and emerging of liquid water were discussed. Numerical models that considered the porous mediums were developed in several ways. Nam and Kaviany [23] developed a two dimensional, two-phase numerical model by considering random carbon fibre mats as the GDL. Single- and two-layer diffusion mediums were both considered to investigate the effective diffusivity and water saturation. A study on the interaction between the GDL and the flow field was performed by Dohle et al. [24] numerically and experimentally. Other models that considered the porous mediums also mainly focused on the porosity of the carbon fibre paper that could influence the performances of PEM fuel cells [25,26]. However, the detailed flow patterns that liquid water exhibits across the porous medium and the effects of the micro-structures of GDL were rarely discussed.

Some very important facts have often not been paid serious attention: the conventional GDLs are not effective for water removal. This is because the micro-structure and the size of the pores of conventional GDLs are very arbitrary, and the sizes of the pores are very small (10 and 30 μm). Due to the physical features of the conventional GDLs, it is very frequent for liquid water to flood the GDL and catalyst layer in practical PEM fuel cells. The main reason causing frequent flooding is that the arbitrary structure of conventional GDLs does not allow a well-organized liquid water flow.

In this paper, different kinds of innovative GDLs, with well-designed micro-flow channels are proposed to solve these problems. And in this paper, to investigate the details of the water removal characteristics of the proposed innovative GDLs and to predict the distribution of liquid water, a unit serpentine gas flow channel with three different kinds of micro-structures of innovative GDLs were studied. Different flow patterns in different micro-structures are presented graphically. In this work, the details of phase change and electro-chemical reaction were not considered. Based on the authors' understanding, the effect of the electro-chemical reaction inside the PEM fuel cell on liquid water behaviour is mainly to continuously supply water. Based on this premise, various operating conditions for a PEM fuel cell could be simulated without involving details of electro-chemical reactions. In the present work, therefore, an initial liquid water distribution was employed to simplify the complex process of real PEM fuel cell operating condition.

In the following, the computation domain, solution procedure and mesh independency are introduced. Then the results and discussions are presented. Finally, conclusions are drawn and some valuable design and optimization related suggestions are given.

2. Numerical model setup

2.1. Computation domains with innovative micro-flow channels of GDL, and boundary conditions

Fig. 1 illustrates the schematics of the computation domains showing the three different domains that were investigated, at the top left side of Fig. 1b–d, the cross sections (the y–z planes) along the center-planes of the porous holes for each computation domain were shown. The computation domains have the same U-shaped channel—the unit of a serpentine PEM fuel cell flow channel, with dissimilar GDL designs. The gas flow channel has a cross section of 1 mm × 1 mm along the y- and z-direction. Each straight section of the gas flow channel is 15 mm long. On the membrane electrolyte assembly (MEA) side, small paths with different kinds of geometry are used to represent the holes on different GDLs: 0.1 mm × 0.1 mm × 0.1 mm cubes are used for the GDLs in computation domain 1; trapezoids with the height of 0.1 mm along the z-direction, and the minimum area (0.1 mm × 0.1 mm along the x- and y-direction) facing the catalyst layer are used for the GDLs in computation domain 2; the same trapezoids but with the minimum area facing the gas flow channel are used for the GDLs in computation domain 3. In order to keep the flow rate across the holes identical, the

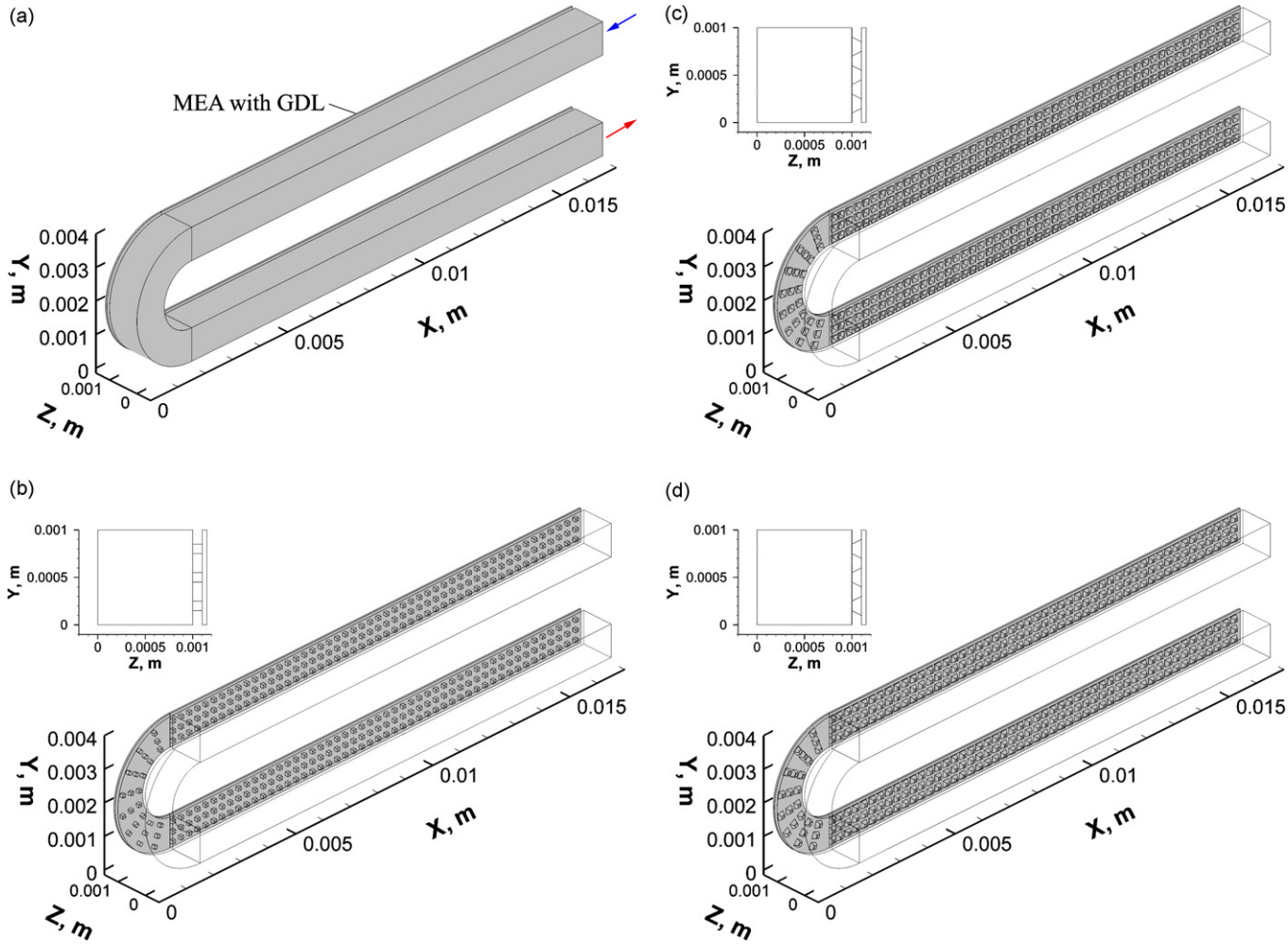

Fig. 1. Computation domains: (a) general view; (b) computation domain 1; (c) computation domain 2; (d) computation domain 3.

minimum cross sections are the same for all the computation domains (0.1 mm × 0.1 mm along the *x*- and *y*-direction). The location and amount of the holes are also identical for all the computation domains.

As mentioned in the introduction, the conventional GDLs are not effective for water removal due to the random nature of its micro-structure and small pore size (10–30 μm). Therefore, three innovative micro-structures have been proposed in this paper, as shown in Fig. 1b–d. Here all "pores" are well designed and structured, i.e., well-structured small holes (micro-flow channels) connecting the gas flow channel and catalyst layer as shown in Fig. 1b–d. Furthermore all the computation domains have the same gap of 0.05 mm between the GDLs and the membranes/catalyst layers. To simplify the numerical model, and because the purpose of this study is to investigate how the liquid water flows through different designs of GDLs into the gas flow channels, the gaps between the GDLs and the membranes/catalyst layers were set to be non-porous, this is corresponding to the extreme case for 100% water flooding inside the catalyst layer of a PEM fuel cell.

The isothermal air–water transport process inside the computation domain was modeled as a 3D two-phase viscous laminar flow. A no-slip boundary condition was applied to the surrounding walls. A Velocity Inlet boundary condition (uniform air velocity distribution of 10 m s^{-1} with a direction normal to the inlet boundary) was applied at the air inlet of the upper section of the U-shaped channel. At the outlet, the boundary condition was assigned as outlet flow (the gradients of all flow properties are zero). Gravity was taken as being along the negative *y*-direction. To simulate water removal characteristics of different GDLs, an initial water distribution inside the computation domains was carefully set up and the details are given in Section 3.

2.2. Computational methodology

The numerical simulations of the 3D, unsteady, laminar, two-phase flow in the computation domain was performed using FLUENT [27]. An inspection of the numerical setup revealed that the Reynolds number in the model was less than 700, thereby verifying laminar flow assumption. No energy equations were considered thus the conservation of mass and momentum were the governing equations for the model. To track the air–water two-phase flow interface inside the computation domain, the volume-of-fluid (VOF) [27] method implemented in FLUENT was used. The VOF model is designed for two or more immis-

cible fluids, where the position of the interface between fluids is of interest.

Then the conservation laws of mass and momentum governing unsteady, laminar flow could be written as [27]:

- Continuity equation:

$$\frac{\partial \rho}{\partial t} + \nabla \cdot (\rho \vec{v}) = 0 \tag{1}$$

- Momentum equation:

$$\frac{\partial(\rho\vec{v})}{\partial t} + \nabla \cdot (\rho\vec{v}\vec{v}) = -\nabla p + \nabla \cdot [\mu(\nabla\vec{v} + \nabla\vec{v}^{\mathrm{T}})] + \rho g + \vec{F} \tag{2}$$

where p is the static pressure and $\vec{F}$ is the surface tension force.

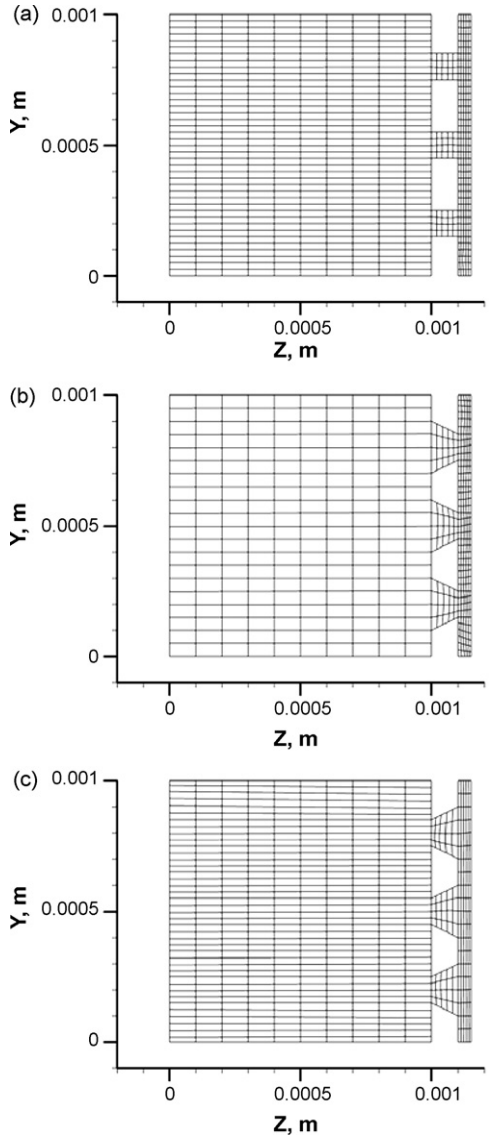

Fig. 2. Meshes on y–z planes: (a) computation domain 1; (b) computation domain 2; (c) computation domain 3.

Volume fraction of liquid water (α^2) could be solved by

$$\frac{\partial \alpha_2}{\partial t} + \vec{v} \cdot \nabla \alpha_2 = 0 \tag{3}$$

Then the volume fraction of air (α_1) could be calculated by using the relation:

$$\alpha_1 + \alpha_2 = 1 \tag{4}$$

All the other properties (e.g., viscosity) could be computed in a volume-fraction weighted-average manner as

$$\mu = \alpha_2\mu_2 + (1 - \alpha_2)\mu_1 \tag{5}$$

In the FLUENT simulation package, the surface tension is considered as a source term in the momentum equation. For two phase flow, it can be expressed as

$$F_{\mathrm{vol}} = \sigma_{12}\frac{\rho\kappa_1\nabla\alpha_1}{(1/2)(\rho_1 + \rho_2)} \tag{6}$$

where F_{vol} is the source term of the surface tension in momentum equation, σ_{12} the surface tension coefficient, ρ the volume-averaged density and κ is the surface curvature of at the interface between two phases.

2.3. Validation of grid independency

There were 821,520, 423,720, and 622,620 cells meshed in computation domains 1, 2, and 3, respectively. Fig. 2 shows the meshes on y–z planes for the three computation domains. Each cell in the straight channel sections had the same size with dimensions of 0.025 mm × 0.025 mm × 0.1 mm (along x, y, and z directions, respectively) for computation domain 1, 0.05 mm × 0.05 mm × 0.1 mm for computation domain 2, and 0.025 mm × 0.025 mm × 0.1 mm for computation domain 3. Trapeziform cells were employed to generate the corners of the serpentine gas flow channels. In the porous sections, for all the computation domains, the holes were divided into four sections along the x- and y-direction, and five sections along the z-direction. The dimensions of the cells along the z-direction are 0.02 and 0.01 mm for the GDLs and the membranes/catalyst layers, respectively. This size was also identical for all the three computation domains. Grid independency was tested by

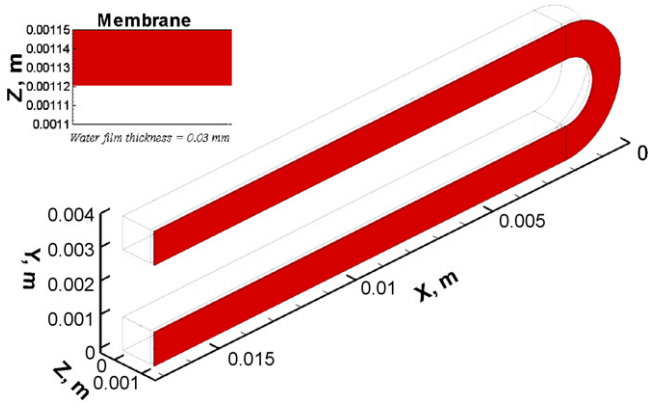

Fig. 3. Initial water distribution.

Table 1
Three simulated cases for different computation domains and PEM fuel cell operating condition

Case no.	Computation domain no.	Inlet velocity ($m\,s^{-1}$)	Initial film thickness (mm)	Initial water (mm^3)	Initial water distribution	Corresponding PEM fuel cell operating condition
1	1	10	0.03	1.04	Water films with a thickness of 0.03 mm placed on membrane/catalyst layer	Water flooding for case with proposed GDL shown in Fig. 1b
2	2	10	0.03	1.04	Water films with a thickness of 0.03 mm placed on membrane/catalyst layer	Water flooding for case with proposed GDL shown in Fig. 1c
3	3	10	0.03	1.04	Water films with a thickness of 0.03 mm placed on membrane/catalyst layer	Water flooding for case with proposed GDL shown in Fig. 1d

both doubling and halving of grid cells for all the computation domains. The flow phenomena of liquid water and the velocity field were almost the same. The difference in results for the different mesh systems was so small that it is negligible.

3. Results and discussion

In order to investigate two-phase flow behaviour across the GDLs, three different cases corresponding to different computation domains were simulated as listed in Table 1. A liquid water film was initially placed on the membranes to investigate the water removal characteristics. Fig. 3 shows the arrangement of the initial water distribution. Detailed results and discussions are given below.

3.1. Case 1: water films with a thickness of 0.03 mm placed on membrane/catalyst layer for computation domain 1

The first case was simulated to investigate the effects of the GDLs with cubic micro-structures on liquid water flow

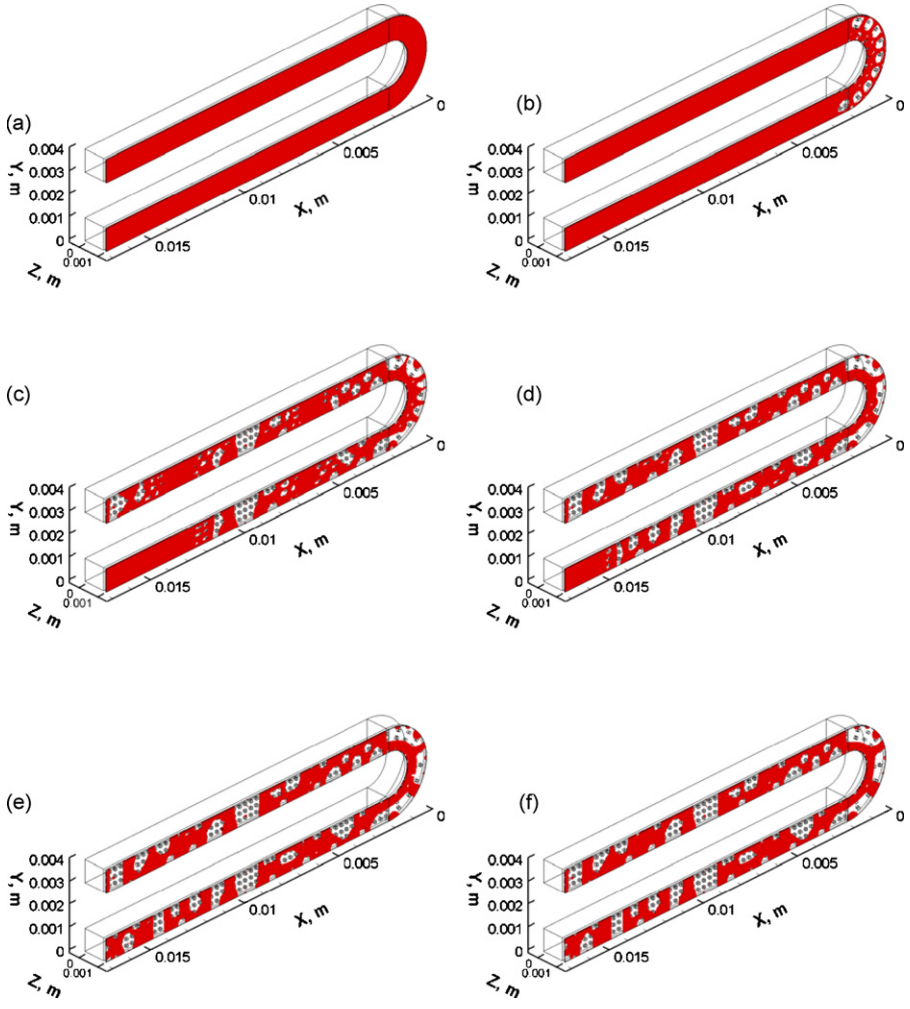

Fig. 4. Abruption of water films in 3D view for Case 1: (a) $t = 0$ s; (b) $t = 0.0005$ s; (c) $t = 0.003$ s; (d) $t = 0.005$ s; (e) $t = 0.007$s; (f) $t = 0.02$ s).

behaviour. As shown in Fig. 3, and listed in Table 1, water films with a thickness of 0.03 mm were placed on membrane/catalyst layer in computation domain 1. The abruption of water films, change of water occupation fraction in the MEA, and water transport inside the MEA were studied.

3.1.1. Abruption of water films and its effects on velocity fields

Fig. 4 shows the abruption of the initially attached water films while Fig. 5 depicts the water distribution and velocity field on the center-plane of the catalyst layer. The abruption of the water films started from the corner, as shown from Figs. 4b and 5b. One of the main reasons for the water film to rupture from the corner could be attributed to the strong secondary flows formed at that location. The flow field along the other two directions (the cross section of the main flow direction) became stronger thus breaking up the balance between the air flow and the water films. Detailed descriptions of this kind of flow phenomena were discussed in the authors' previous publications [18,19]. By comparing Figs. 6–9, the enhancement of the secondary flow could also be observed. In the cross sections close to the serpentine corner (Figs. 6 and 7, $x = 0.00205$ m), the secondary flow is much stronger than at the cross sections further away from the corner (Figs. 8 and 9, $x = 0.01105$ m). Because of the formation of the abruptions, some of the porous holes at the corner were not facing the water films. This leads to a decrease in the flow resistance at those holes facing the abruptions and subsequently breaking up the balance between air and water from these sections. As a result, more air could flow through these holes into the catalyst layer., The velocity at the corner, therefore, increased and the air started flowing from the emptied sections to both of the straight sections at the inlet and outlet, as observed from Fig. 5 b, at $t = 0.0005$ s. As shown in Figs. 10 and 11, water distribution and velocity field on the center-plane in both of the inlet and outlet sections at the serpentine corner could be observed (please note that the vertical lines in the gas flow channel and the catalyst layer at $x = 0.002$ m do not represent walls, these lines only represent the joints of the serpentine sections and the straight sections, they are all interiors). As shown in Fig. 10a, for the inlet straight section at $t = 0.0001$ s, the initially attached flat water films were in wave-form, especially in the corner. Then, at $t = 0.0002$ s (Fig. 10b), the first abruption was formed at the corner. It could be noticed that the main flow in the catalyst layer is along the positive x-direction while it is along the negative x-direction in the flow channel. The air was taking the water from the abruptions towards the straight section, and the effects of the main flow direction in the gas flow channel were insignificant. A similar condition could be observed in Fig. 11a and b. Abruptions formed and water started flowing towards the straight section but along the same direction as the main flow in the flow channel. However, this is not due to the effect of the main flow, as mentioned.

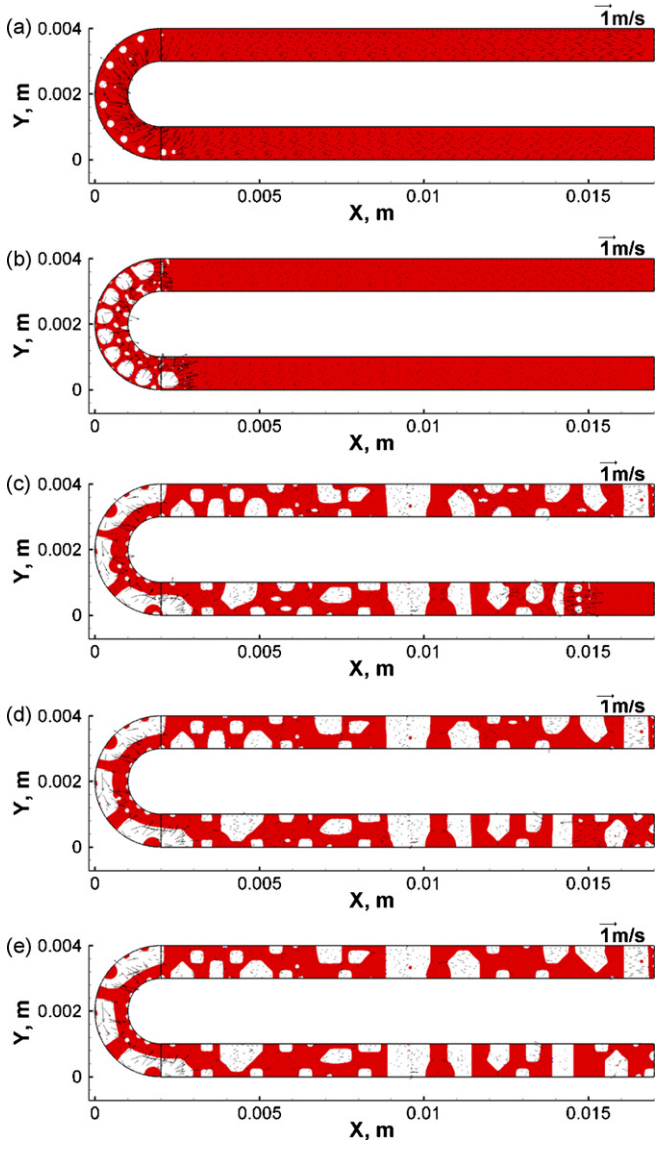

Fig. 5. Water distribution and velocity field on the center-plane ($z = 0.001125$ m) in the membrane/catalyst layer for Case 1: (a) $t = 0.0001$ s; (b) $t = 0.0005$ s; (c) $t = 0.005$ s; (d) $t = 0.007$ s; (e) $t = 0.02$ s).

At the air flow inlet, because the air flow was not fully developed, the air flow around the boundaries was stronger than that of the fully developed flows further from the inlet. Stronger air flow was formed across the porous holes close to the inlet, thus breaking up the balance between the air and water, and abruptions were formed as well. Fig. 12 shows the detailed process on the center-plane at the inlet section. At $t = 0.001$ s (Fig. 12a), the deformation of the water film could be observed, and then at $t = 0.0011$ s (Fig. 12b), the deformation increased and stronger air flow was formed across those porous holes. Abruptions were formed and strong air streams were flowing across the porous holes into the catalyst layer at $t = 0.0012$ s (Fig. 12c). Later on, those air streams started moving the liquid water in the catalyst layer along the negative x-direction, and more abruptions were formed from the initial raptures, as shown in Fig. 12d and e.

As mentioned, the abruptions of liquid water films were formed at the corner due to the stronger secondary flow and the inlet due to the developing flow. Air started moving from those abruptions towards the rest of the un-ruptured water films. The whole process could be observed in 3D view from Fig. 4.

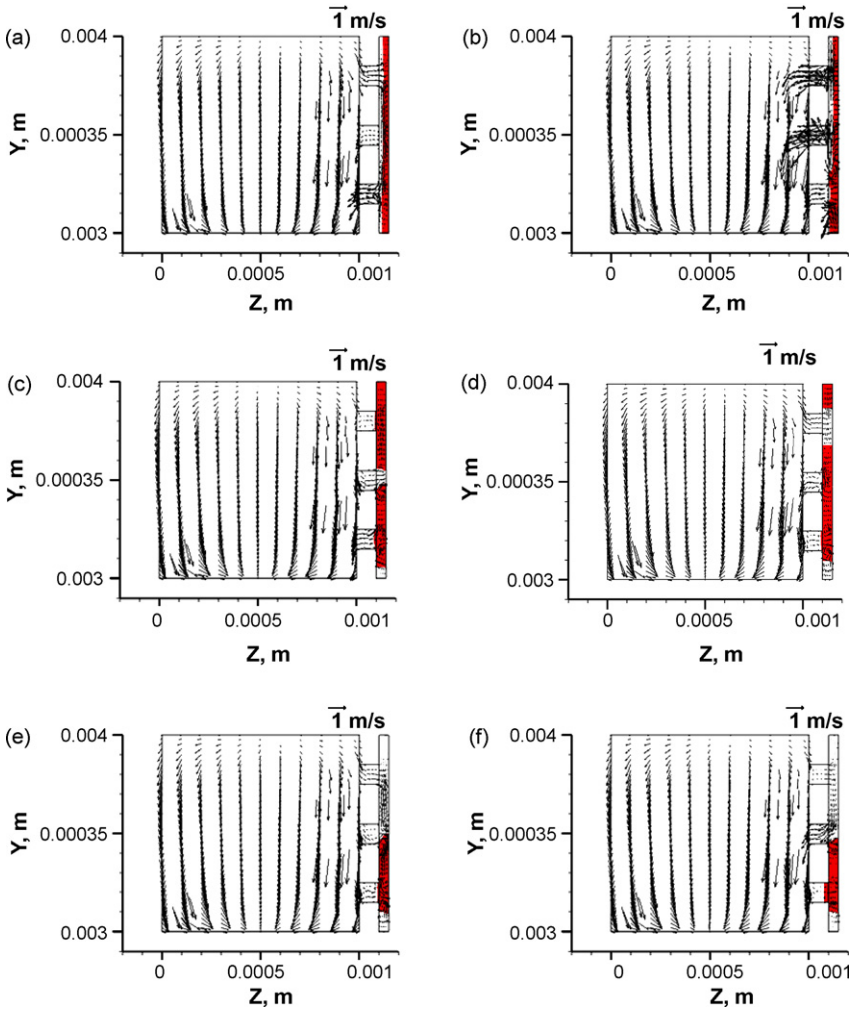

Fig. 6. Water distribution and velocity field on the plane at $x = 0.00205$ m in inlet section for Case 1 ((a) $t = 0.0001$ s; (b) $t = 0.0005$ s; (c) $t = 0.001$ s; (d) $t = 0.002$ s; (e) $t = 0.003$ s; (f) $t = 0.02$ s).

Fig. 5 presents the water distribution and velocity field on the center-plane of the catalyst layer. At $t = 0.003$ s, as shown from Fig. 4, for the inlet straight section (upper section), the water film was broken up from both the inlet and the corner, and for the outlet straight section (lower section), water film was only broken up from the corner. At $t = 0.005$ s, the whole water film in the inlet straight section was ruptured while there was still a small part left in the outlet straight section, which is close to the gas flow outlet. For the straight section at the inlet, even though the ruptures occurred from the both ends, the rupture that occurred from the corner (from $t = 0.0001$ s) was earlier than that from the inlet ($t = 0.0013$ s). In real operating conditions, the flow fields in most parts of the gas flow channels are fully developed, therefore, the abruption of water films at the corner and the spreading to both of the straight sections are the most important flow phenomena that should be considered. By comparing Figs. 6–10, for the cross sections of both straight sections, it could also be observed that on the cross sections closer to the corner ($x = 0.00202$ m), the rupture occurred earlier ($t = 0.001$ s) than on the cross sections further from the corner ($x = 0.01102$ m, $t = 0.002$ s). It can be observed that the spreading speeds of the abruptions along both straight sections were almost the same (the outlet straight section was slightly faster). This could prove that the effect of the flow direction inside the gas flow channel on the flow direction in the catalyst layer is very small because the flow direction inside the catalyst layer is mainly dominated by the water distribution (flowing from empty sections towards liquid water).

After a period of time, as shown from Figs. 4e, f and 5d, e, all the water films were broken up into different pieces. It could be observed that since $t = 0.007$ s, most of the water was no longer moving. The velocity field achieved steady-state and the balance between air and liquid water was attained, which means, all the forces between the two phases, such as surface tension, viscous stresses, wall adhesions etc. were balanced. For example, as shown in Fig. 5e, at the corner, it could be observed that air was flowing from the empty sections to the liquid water. The liquid water was surrounding the inner boundary of the serpentine corner and there was no path for the liquid water to flow elsewhere. This part of liquid water therefore achieved a balance of the forces. When the balance was achieved (no significant movement of liquid water could be observed),

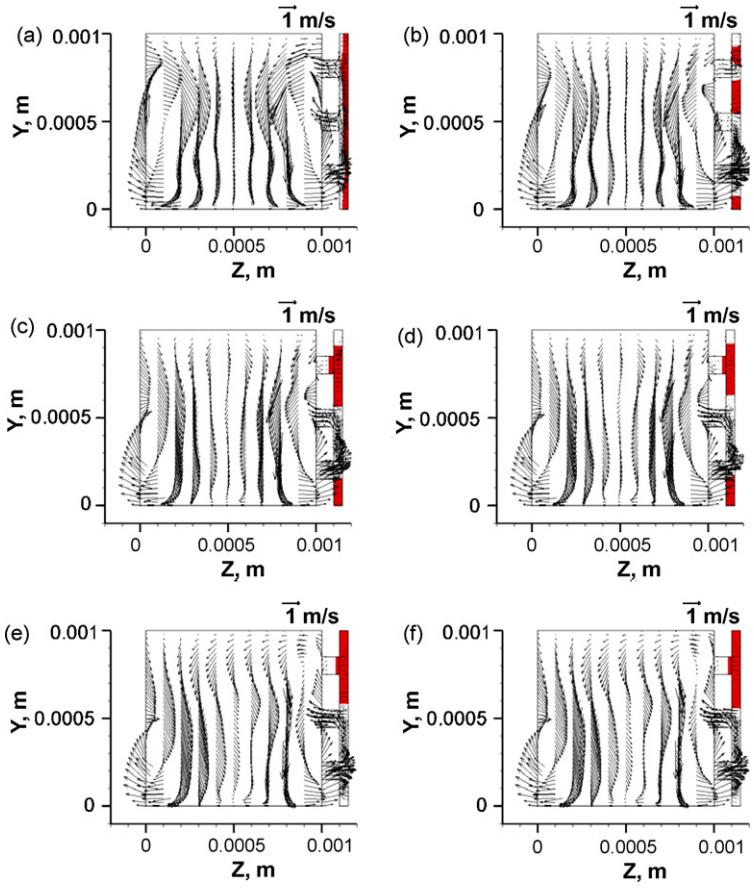

Fig. 7. Water distribution and velocity field on the plane at $x = 0.00205$ m in outlet section for Case 1 ((a) $t = 0.0001$ s; (b) $t = 0.0005$ s; (c) $t = 0.001$ s; (d) $t = 0.002$ s; (e) $t = 0.007$ s; (f) $t = 0.02$ s).

as shown in Fig. 5e, there was almost no liquid water isolated from the surrounding walls. Almost all the liquid water was connecting to the surrounding walls to achieve the force balance.

From Figs. 6f, 7f and 8f, at $t = 0.02$ s while the force balance was achieved, water had difficulties staying between two porous holes and such places suffered air streams flowing from the surrounding holes. Therefore, it is challenging for such places to maintain liquid water, which is good for water drainage. On the other hand, those places around the surrounding wall, which maintained most of the liquid water, are not good for water drainage. In real PEM fuel cell operating conditions, if a whole piece of MEA was considered, these surrounding walls as shown from Fig. 5e, would be connecting to the catalyst layer under the lands of the bipolar plates. Such places are the ideal destinations that the liquid water should move to. Therefore, it could be concluded that for the catalyst layer, the areas under the lands of the bipolar plate and those close to the surrounding walls are the most possible places that liquid water would move to. Other locations that suffer strong air flow and are not surrounded by any walls are relatively difficult in maintaining liquid water.

Fig. 13 shows the water distribution and velocity fields on the x–y planes at both ends of the catalyst layer after the balance between air and liquid water was achieved ($t = 0.02$ s). It could be observed that the water distributions on these two planes were almost the same. The plane closer to the GDL (Fig. 13a) contained slightly smaller amounts of water because it is closer to the air flow. Additionally, by considering Fig. 5e which shows the plane between them at the same time, very similar water distribution could be observed. Therefore, it could be concluded that liquid water inside the catalyst layer would tend to reach a force balance by touching both the top and bottom surfaces. This is the most stable condition for liquid water because the force due to the wall adhesion effects is the maximum and the effect of the surface tension between air and liquid water is the minimum.

3.1.2. *Water occupation fraction variation*

Fig. 14 shows the water occupation fraction (the average volume fraction of water) inside the MEA for Case 1. It was observed that the total water occupation fraction inside the MEA only decreased from 50.4 to 44.9% i.e. only a very small amount of water was removed. It was observed that the water amount inside straight sections of the MEA even increased. This is because liquid water inside the corner moved into those straight sections, as mentioned above. At the beginning, the water occupation fraction inside the straight sections reached the maximum. This is because in that time period, the rate of liquid water moving into those sections from the corner was higher

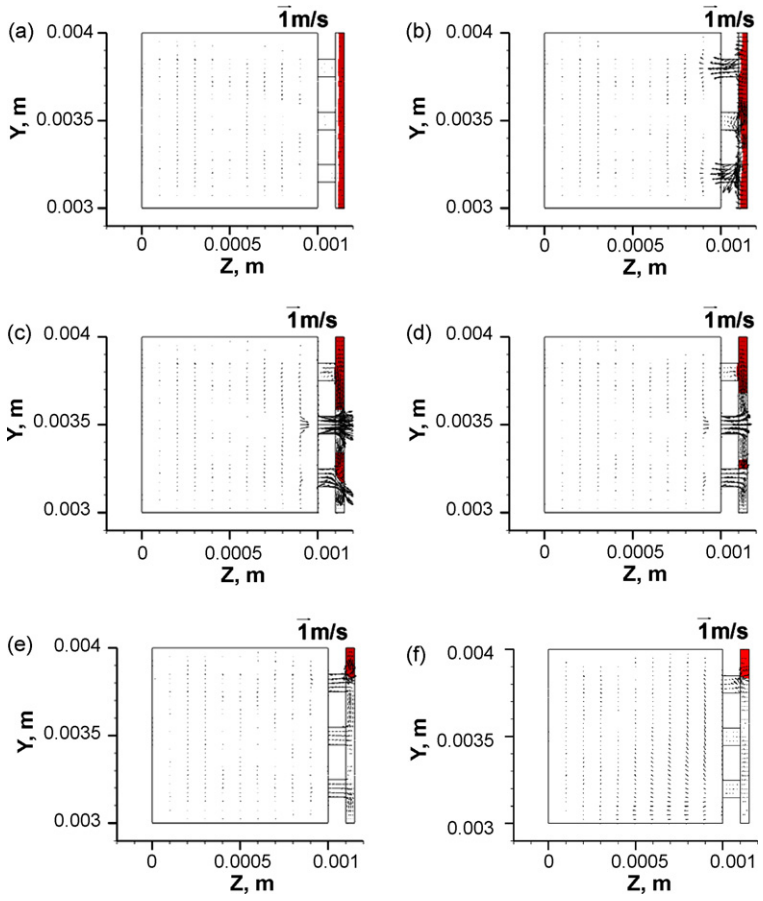

Fig. 8. Water distribution and velocity field on the plane at $x = 0.01105$ m in inlet section for Case 1 ((a) $t = 0.001$ s; (b) $t = 0.002$ s; (c) $t = 0.0022$ s; (d) $t = 0.0025$ s; (e) $t = 0.003$ s; (f) $t = 0.02$ s).

than the rate of water moving out. Later on, a slight reduction of water occupation fraction inside those straight sections could be observed; because at that time the abruption of liquid water films at the corner was complete and water movement relatively decreased. After the balance was achieved, the water occupation fraction inside the straight sections became almost constant. Furthermore, water occupation fraction inside the straight section at the inlet was larger than at outlet (the total volume of these two sections are the same). This could be explained with the help of Fig. 5b, at $t = 0.0005$ s, as the water films ruptured at the corner, it could be noticed that water films also ruptured from the left side of the straight section at outlet, close to the corner. Such abruption was, however, not observed at the inlet straight section. This is because as air flowed through the corner, the secondary flow was still very strong although air already flowed into the straight section. The comparison of the secondary flow before entering the corner and after exiting could be noticed in Figs. 6 and 7. Fig. 7 (for the outlet section) showed stronger secondary flow than Fig. 6 (for the inlet section). Therefore, water films ruptured from the left side of the straight section at outlet first, at the strong air flow formed there could prevent some water flowing from the corner, thus explaining why the straight section at inlet contained more water. It could also be observed that the straight section at inlet reached a constant water occupation fraction earlier than at outlet. This is because for the straight section at inlet, abruptions occurred from the both ends (as mentioned, also from the inlet due to the developing flow), thus the abruptions developed faster than the straight section at outlet. The highest reduction of water occupation fraction could be observed at the corner, which was only 9% by comparing its original water occupation fraction at 54%. The strong secondary flow at the corner did not help removing the water significantly, and the 9% even contained some water flowed into the straight sections.

Fig. 15 shows the water occupation fraction inside the catalyst layer for Case 1. This figure showed a very similar water variation to that shown in Fig. 14. However, in the catalyst layer, water occupation fractions inside the straight sections were finally less than the initial condition. This is because some water moved into the GDL. Fig. 16 shows the water occupation fraction inside the GDL for Case 1. As mentioned above water was only removed significantly at the corner, however, the porous holes contained the most water at the corner and the straight section at inlet contained the least. The reason that the GDL also contained some water after the balance was achieved is as discussed above. All the water was finally connecting to the both ends of the catalyst layer and the water could also be able extend into the GDL and remain balanced due to water's viscosity. Such phenomena could be observed in Figs. 6 and 7.

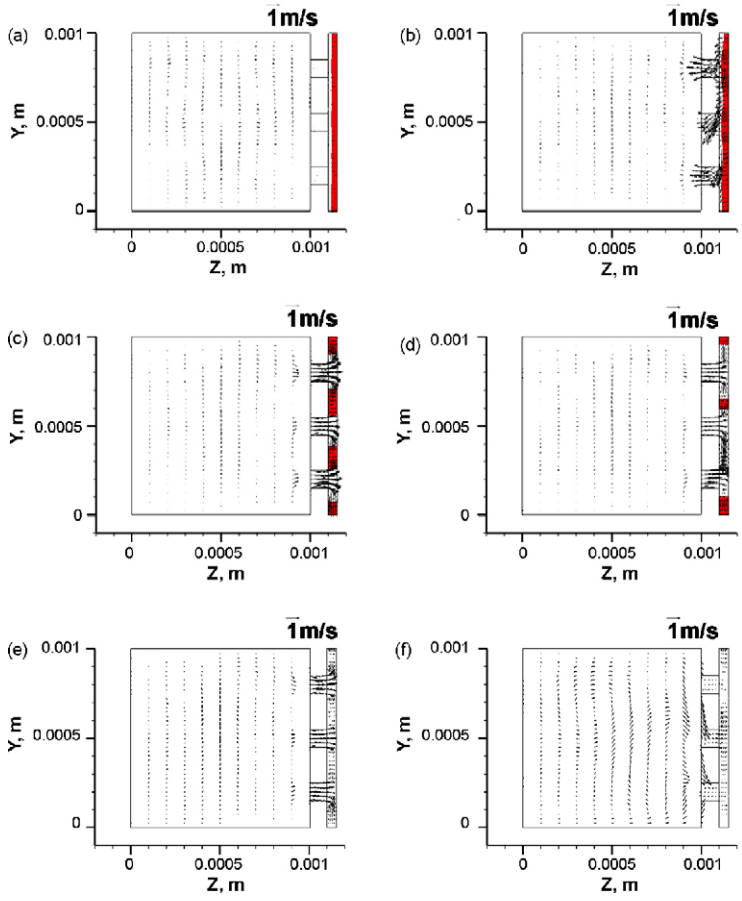

Fig. 9. Water distribution and velocity field on the plane at $x = 0.01105$ m in outlet section for Case 1 ((a) $t = 0.001$ s; (b) $t = 0.002$ s; (c) $t = 0.0022$ s; (d) $t = 0.0025$ s; (e) $t = 0.003$ s; (f) $t = 0.02$ s).

It could be concluded that the secondary flow is still strong after exiting the serpentine corner; therefore, the water was easier to be removed after air exits from the corner than before air enters the corner. Even though water was removed faster at the corner, some parts of the water did not flow into the flow channel but flowed into other parts of the MEA, which is still not good for PEM fuel cell performance. The more water removed from the catalyst layer, the more possibility that the GDL contains more water. The regular cubic micro-structure of the GDL is not good for water removal as only 0.5% of the total volume was removed with this structure.

3.2. Case 2: water films with a thickness of 0.03 mm placed on membrane/catalyst layer for computation domain 2

The second case was simulated to investigate the effects of the GDLs with trapeziform micro-structures on liquid water flow behaviour. The trapeziform porous holes in computation domain 2 (Fig. 1c) had a height of 0.1 mm along the z-direction with the minimum area (0.1 mm × 0.1 mm along the x- and y-direction) facing the catalyst layer. As shown in Fig. 3, and listed in Table 1, water films with a thickness of 0.03 mm were placed on the membrane/catalyst layer in computation domain 2. The abruption of water films, change of water amount in the MEA, and water transport inside the MEA were studied.

3.2.1. Abruption of water films and the effects of the GDLs with trapeziform micro-structures (the minimum area facing the catalyst layer) on liquid water transport

The only difference between the first two cases is the shape of the porous holes. As shown in Fig. 17, it could be noticed that the general water transport phenomena was similar to Case 1. The abruption of water films started at the corner and the inlet with the balance between air and water achieved after all the liquid water films ruptured. Liquid water would stay around the end walls in the catalyst layer and almost all the liquid water would connect the both ends of the catalyst layer (the membrane side and the GDL side). Fig. 18 shows the cross section on the y–z planes close to the corner. It was noticed that the secondary flow in the plane at the downstream of the corner was stronger than at the upstream (also shown in Case 1).

Even though the general flow characteristics between the first two cases were similar, the water flow behaviours inside the MEA were still different. By observing Figs. 17–20, no water was flowing into the GDL and thus the water removal ability was even weaker than in Case 1. As shown in Figs. 19 and 20, the

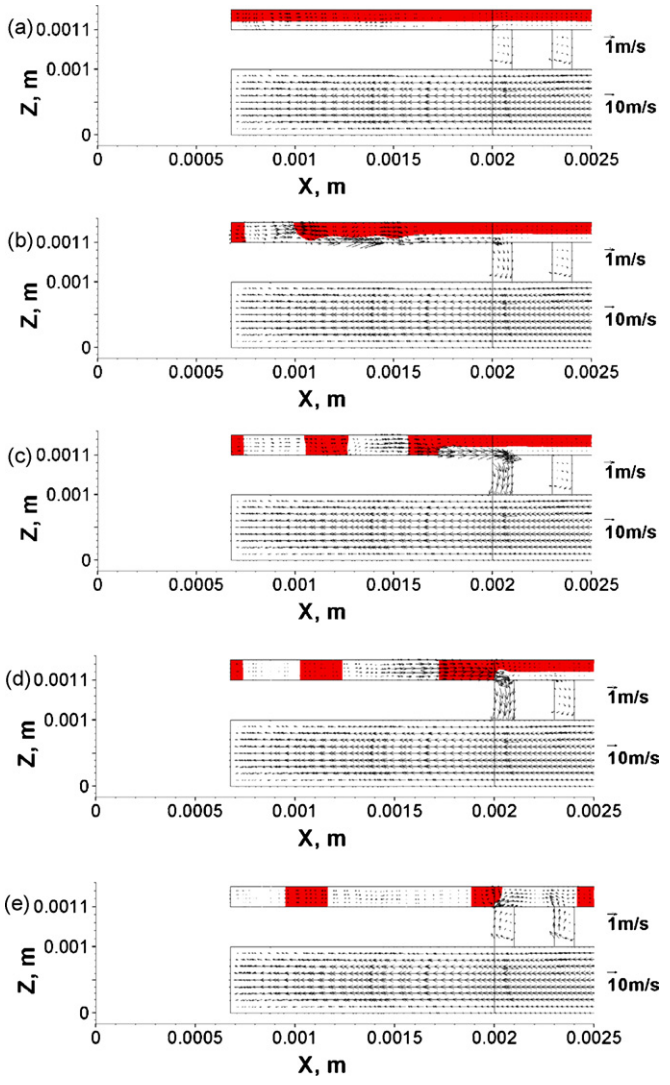

Fig. 10. Water distribution and velocity field on the center-plane ($y = 0.0035$ m) in inlet section at the corner for Case 1 (2× magnification along the z-direction for the MEA, 3× minification along the z-direction for the flow channel) ((a) $t = 0.0001$ s; (b) $t = 0.0002$ s; (c) $t = 0.0003$ s; (d) $t = 0.0005$ s; (e) $t = 0.001$ s).

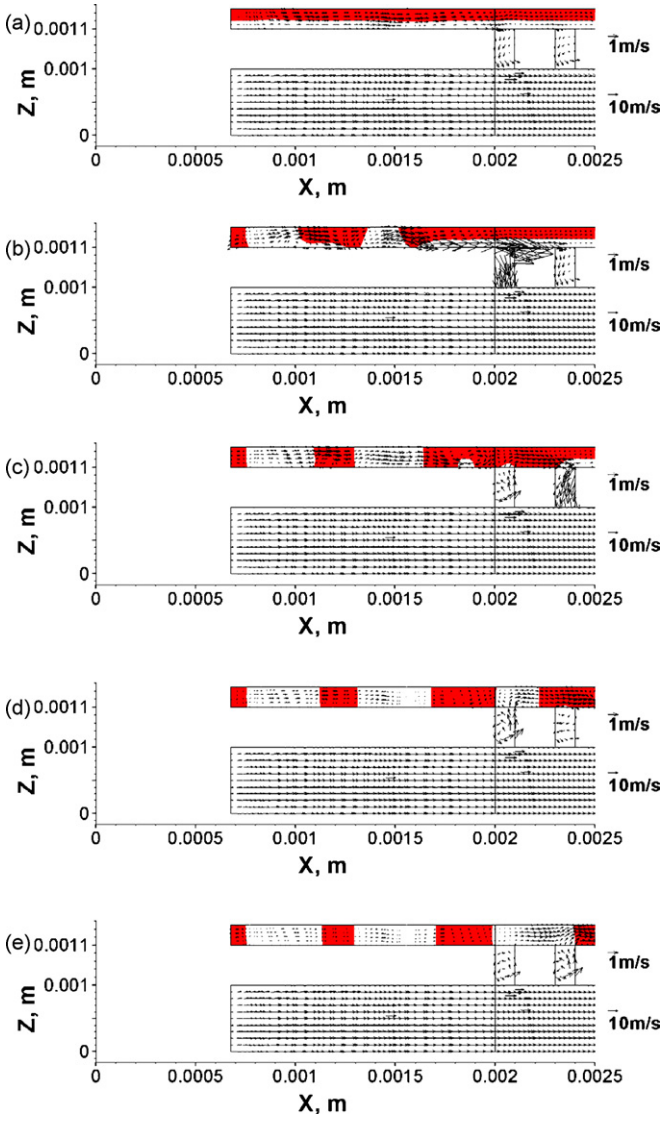

Fig. 11. Water distribution and velocity field on the center-plane ($y = 0.0005$ m) in outlet section at the corner for Case 1 (2× magnification along the z-direction for the MEA, 3× minification along the z-direction for the flow channel) ((a) $t = 0.0001$ s; (b) $t = 0.0002$ s; (c) $t = 0.0003$ s; (d) $t = 0.0004$ s; (e) $t = 0.0005$ s).

water distribution and velocity field on the center-planes of the inlet and outlet sections could be observed. Initially it was the same as in Case 1 in that the water film was broken up into small pieces, however, later on those small pieces did not flow through the porous holes into the gas flow channel. The small pieces of liquid water attached together again to form larger pieces. Such large pieces are difficult to remove and then the balance between air and water was achieved. With the help of Figs. 19 and 20, the reason that the small pieces of liquid water did not flow through the GDL and formed larger pieces could be explained. The micro-structure of the porous holes was trapeziform in this case with the minimum area facing the catalyst layer. While air flowed through these holes, the direction of the flow started concentrating together along the boundary of the holes. Therefore, the flow between two holes in the catalyst layer was weaker than in Case 1. Because such air flow inside the catalyst layer was weak those small pieces of liquid water became easier to attach to each other rather than being broken up and flowed out of the MEA. As seen from Figs. 19 and 20, the air flow between the pieces of liquid water was not strong enough to prevent them from coalescing. Therefore, after a larger piece was formed, the liquid water became even harder to be removed.

3.2.2. *Water occupation fraction variation*

Fig. 21 shows the water occupation fraction inside the MEA for Case 2. It was observed that there was no water flowing out of the MEA. An initial reduction of water at the corner could be noticed, however, a slight increase of water occupation fraction was observed later. This is because initially some water was flowing from the corner to the straight sections but there was no water removed from the MEA. Therefore, after a period of time, some excess water in the straight sections flowed back into the corner. This could be illustrated by the water occupation fraction variation inside the straight sections which, after an initial increase decreased and then reached constant levels.

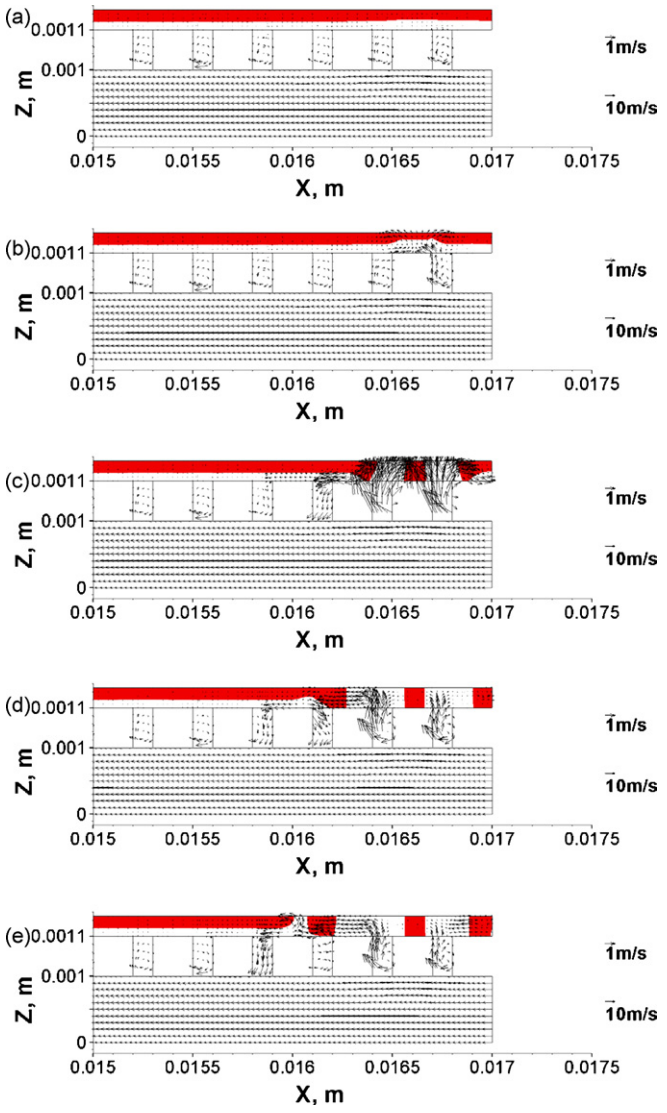

Fig. 12. Water distribution and velocity field on the center-plane ($y = 0.0035$ m) in inlet section at the inlet for Case 1 (2× magnification along the z-direction for the MEA, 3× minification along the z-direction for the flow channel) ((a) $t = 0.001$ s; (b) $t = 0.0011$ s; (c) $t = 0.0012$ s; (d) $t = 0.0014$ s; (e) $t = 0.0015$ s).

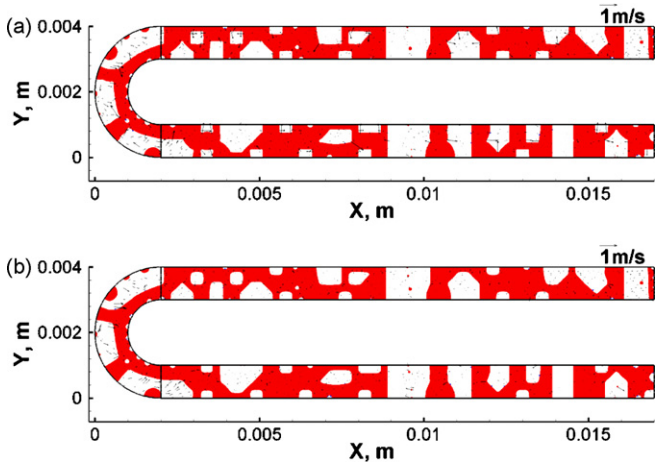

Fig. 13. Water distribution and velocity field on the planes close to the GDL ($z = 0.0011$ m) and close to the membrane ($z = 0.00115$ m) at $t = 0.02$ s for Case 1 ((a) $z = 0.0011$ m; (b) $z = 0.00115$ m).

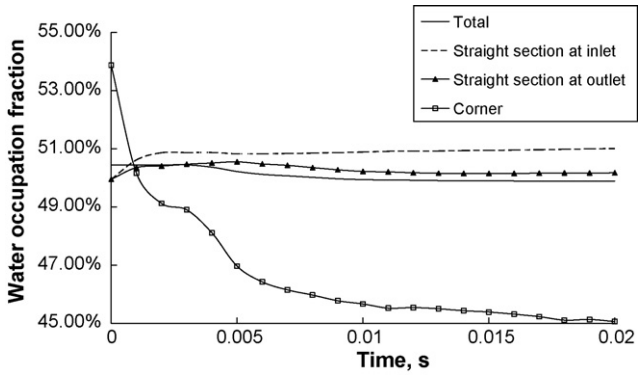

Fig. 14. Water occupation fraction inside the MEA for Case 1.

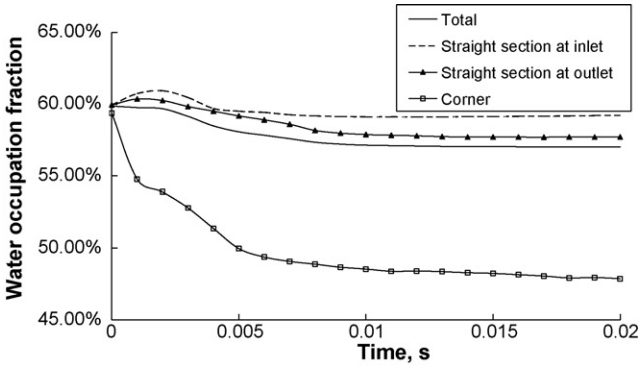

Fig. 15. Water occupation fraction inside the catalyst layer for Case 1.

Because no water was removed from the MEA, in contrast with Case 1, the water occupation fractions in both of the straight sections finally became almost the same. By looking at the water occupation fraction variation inside the catalyst layer in Fig. 22, a 5% reduction of water occupation fraction at the corner was observed. This part of water flowed into the straight sections resulting in a slight increase of water occupation fraction inside the straight sections. Fig. 23 showed that only a small amount of water flowed into the GDL and the water occupation fraction was only about 0.8%. Therefore, most of the water was still inside the catalyst layer.

As mentioned, in comparison with cubic porous holes, the trapeziform micro-structure (with the minimum area

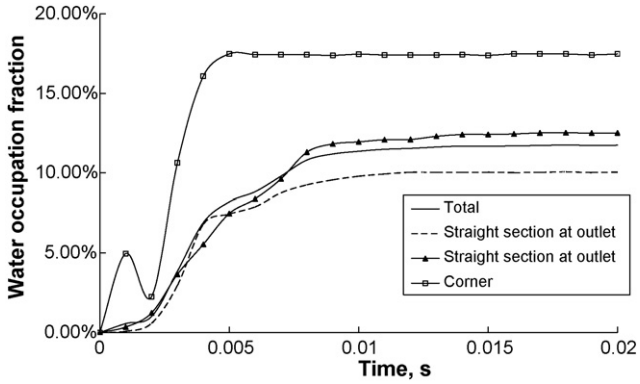

Fig. 16. Water occupation fraction inside the GDL for Case 1.

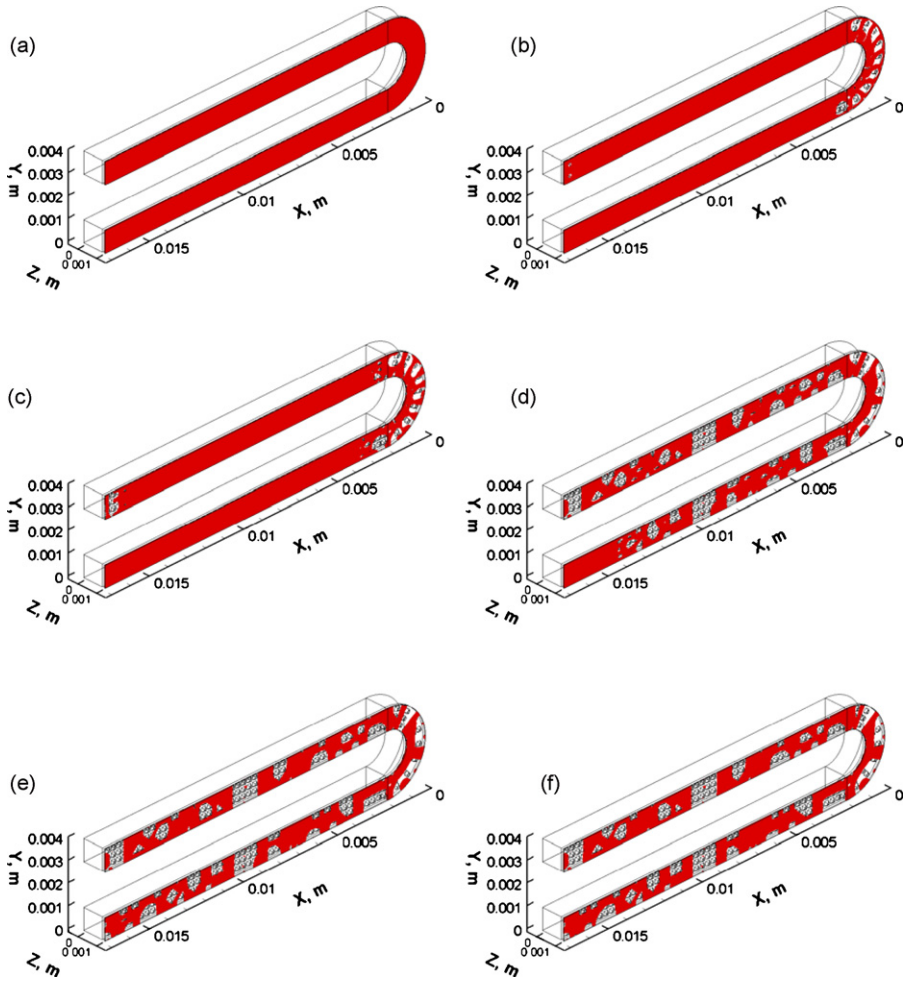

Fig. 17. Abruption of water films in 3D view for Case 2 ((a) $t = 0$ s; (b) $t = 0.0005$ s; (c) $t = 0.001$ s; (d) $t = 0.005$ s; (e) $t = 0.01$ s; (f) $t = 0.02$ s).

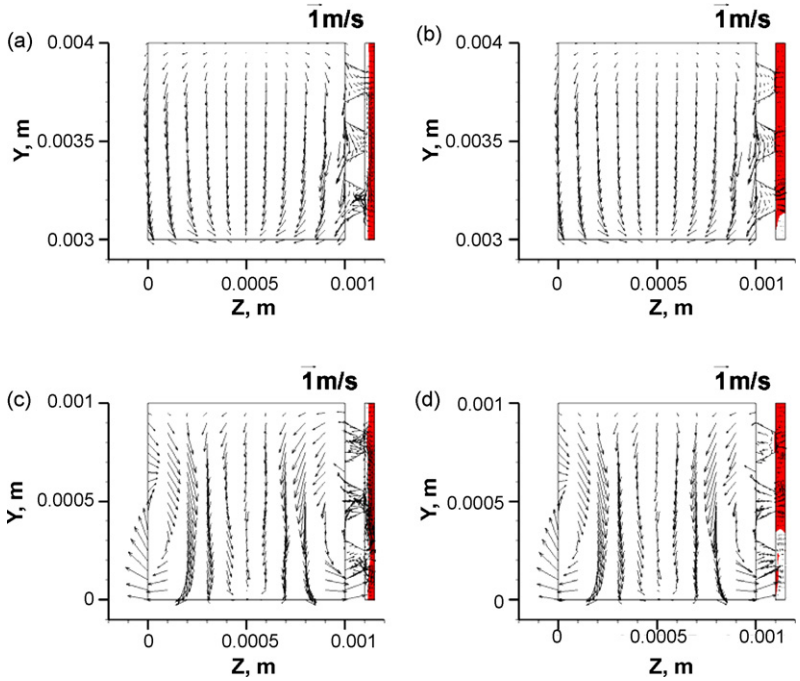

Fig. 18. Water distribution and velocity field on the plane at $x = 0.00205$ m in both inlet and outlet sections for Case 2 ((a) $t = 0.0001$ s at inlet section; (b) $t = 0.02$ s at inlet section; (c) $t = 0.0001$ s at outlet section; (d) $t = 0.02$ s at outlet section).

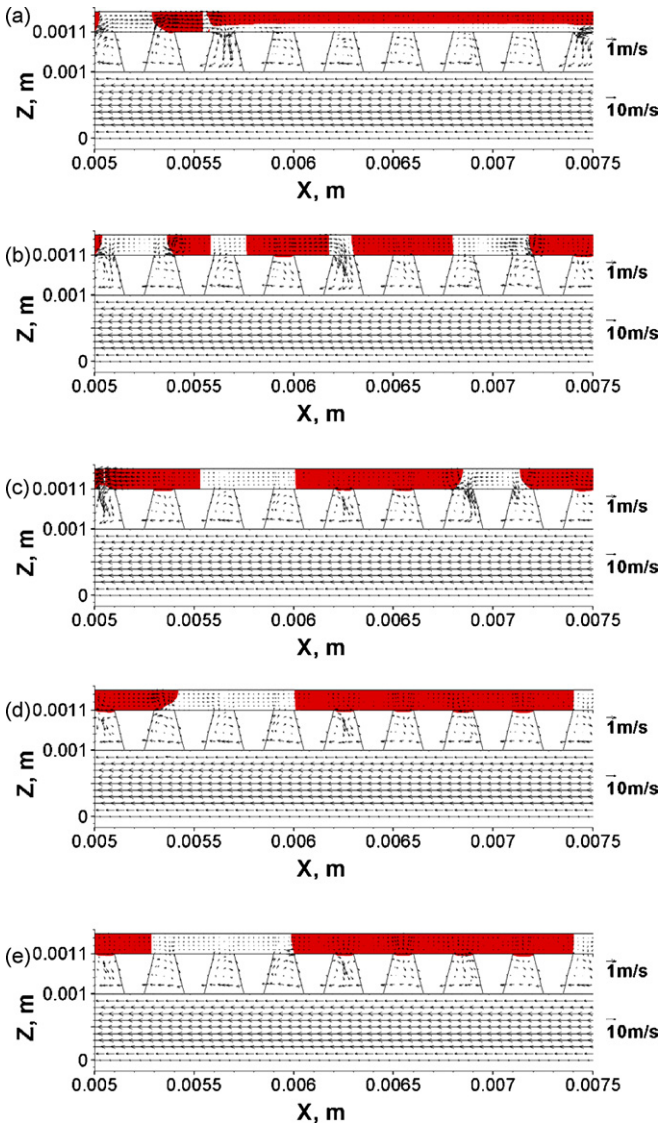

Fig. 19. Water distribution and velocity field on the center-plane ($y = 0.0035$ m) in inlet section for Case 2 (2× magnification along the z-direction for the MEA, 3× minification along the z-direction for the flow channel) ((a) $t = 0.003$ s; (b) $t = 0.004$ s; (c) $t = 0.005$ s; (d) $t = 0.006$ s; (e) $t = 0.02$ s).

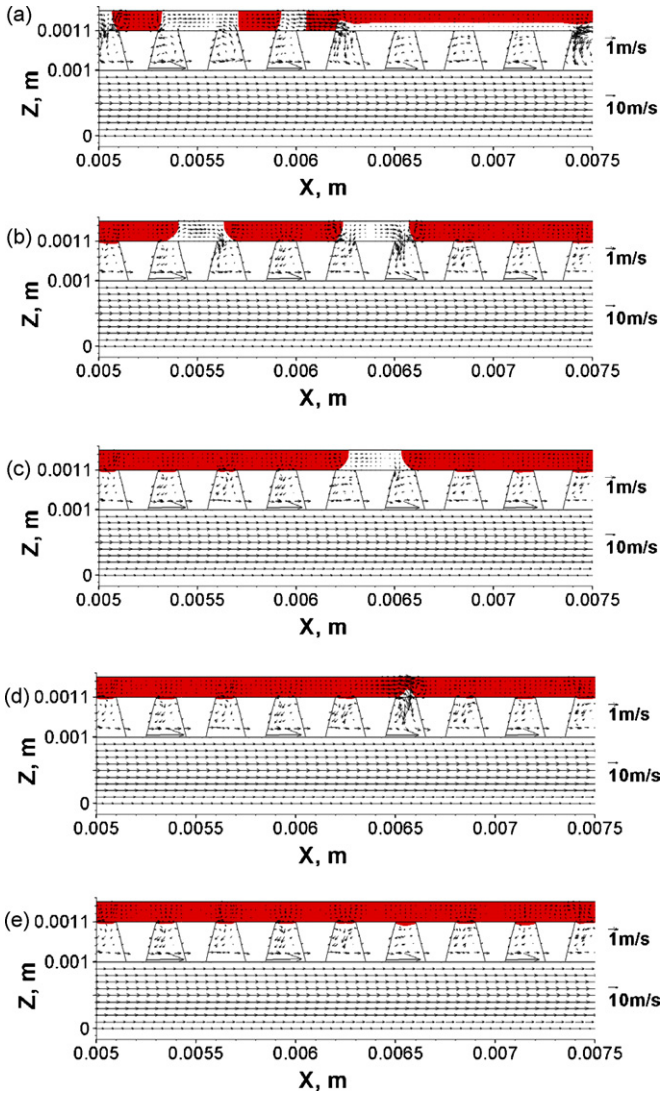

Fig. 20. Water distribution and velocity field on the center-plane ($y = 0.0005$ m) in outlet section for Case 2 (2× magnification along the z-direction for the MEA, 3× minification along the z-direction for the flow channel) ((a) $t = 0.003$ s; (b) $t = 0.005$ s; (c) $t = 0.007$ s; (d) $t = 0.01$ s; (e) $t = 0.02$ s).

facing the catalyst layer) results in a weaker air flow inside the catalyst layer. The water removal ability of such GDL is not acceptable. However, the general flow phenomena are not affected by changing the micro-structures of theGDL.

3.3. Case 3: water films with a thickness of 0.03 mm placed on membrane/catalyst layer for computation domain 3

This case was simulated to investigate the effects of the GDLs with trapeziform micro-structures on liquid water flow behaviour. The trapeziform porous holes in computation domain 3 (Fig. 1d) had a height of 0.1 mm along the z-direction with the minimum area (0.1 mm × 0.1 mm along the x- and y-direction) facing the gas flow channel. As shown in Fig. 3, and listed in Table 1, water films with a thickness of 0.03 mm were placed

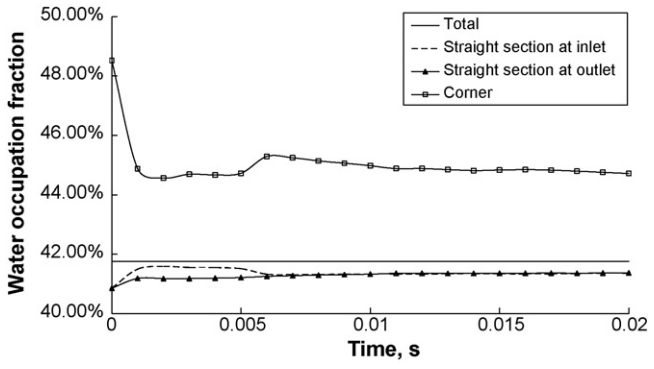

Fig. 21. Water occupation fraction inside the MEA for Case 2.

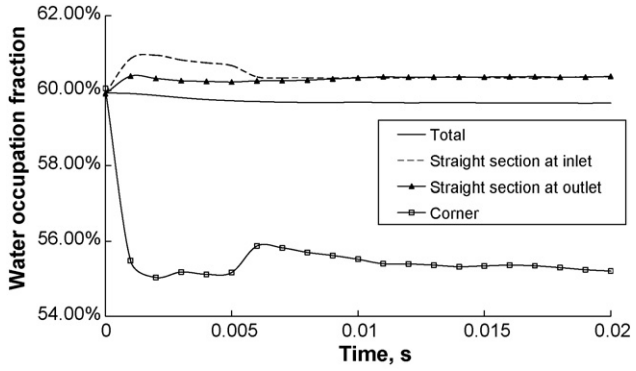

Fig. 22. Water occupation fraction inside the catalyst layer for Case 2.

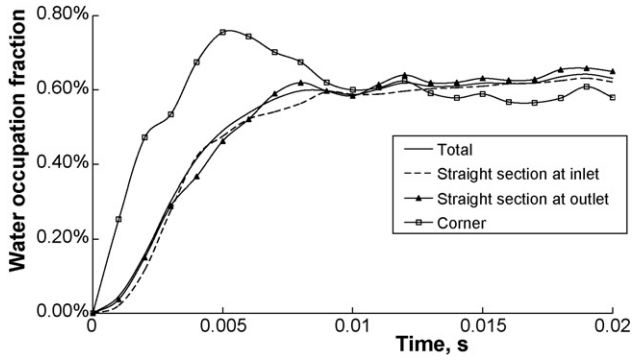

Fig. 23. Water occupation fraction inside the GDL for Case 2.

on the membrane/catalyst layer in computation domain 3. The abruption of water films, change of water amount in the MEA, and water transport inside the MEA were studied. Comparison between the three different micro-structures of GDL was also discussed.

3.3.1. Abruption of water films and the effects of the GDLs with trapeziform micro-structures (the minimum area facing the gas flow channel) on liquid water transport

The general water transport behaviour in this case was similar to Cases 1 and 2. From Fig. 24, the abruption of water films also started from the corner and the inlet. However, after the abruption process was complete the balance between air and water was achieved. The residual water would also tend to stay around the walls in the catalyst layer and connect to the both ends of the catalyst layer. Stronger secondary flow was also observed at the downstream of the corner, as shown in Fig. 25. The only difference between the first three cases is the micro-structures of the GDL. Therefore, it could be concluded that the effects of the micro-structures of the GDL on general liquid water transport serpentine unit cells are insignificant.

However, by observing these figures, a difference in the water amount left could be noticed. The amount of water left in Case 3 was significantly lower than in Cases 1 and 2, Even though the general flow patterns were similar, the flow behaviours of liquid water across the GDL were different i.e. the water removal abilities of different GDLs are different. Fig. 26 shows the liquid water distribution and velocity fields on the center-plane in the outlet straight section. It was observed that during the abruption process, liquid water was separated into small pieces, which was significantly different from Case 2.

As discussed in Case 2, the air flow from the porous holes was relatively localized and the air streams from these holes were not affecting each other. Consequently, the air streams were not strong enough to separate liquid water into small pieces. In this case, the maximum areas of the porous holes were facing the catalyst layer, as shown in Fig. 25. Such flow resulted in air flowing through the porous holes and spreading rather than concentrating into the catalyst layer. Therefore, air streams

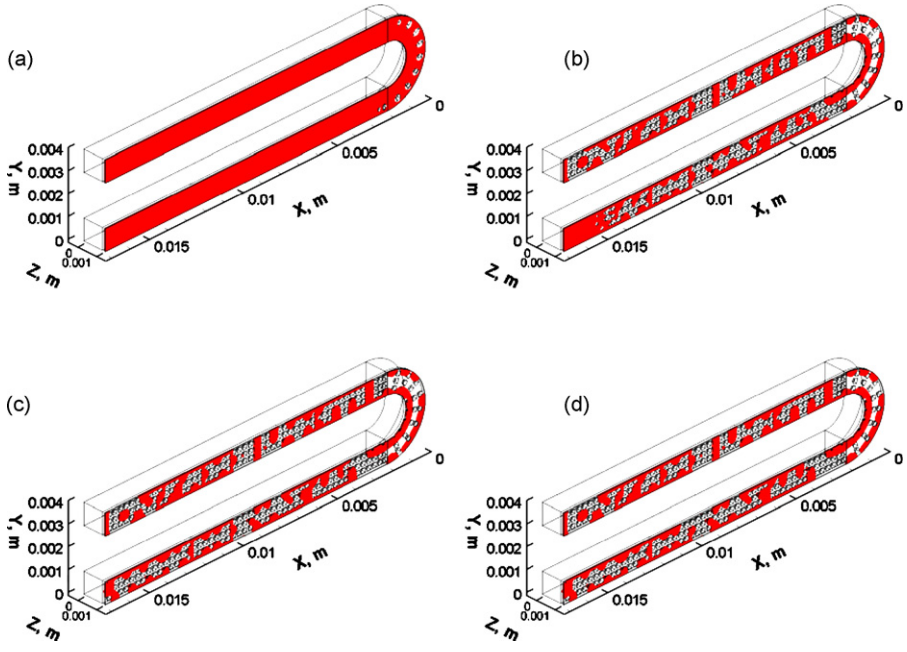

Fig. 24. Abruption of water films in 3D view for Case 3 ((a) $t = 0.0002$ s; (b) $t = 0.005$ s; (c) $t = 0.01$ s; (d) $t = 0.02$ s).

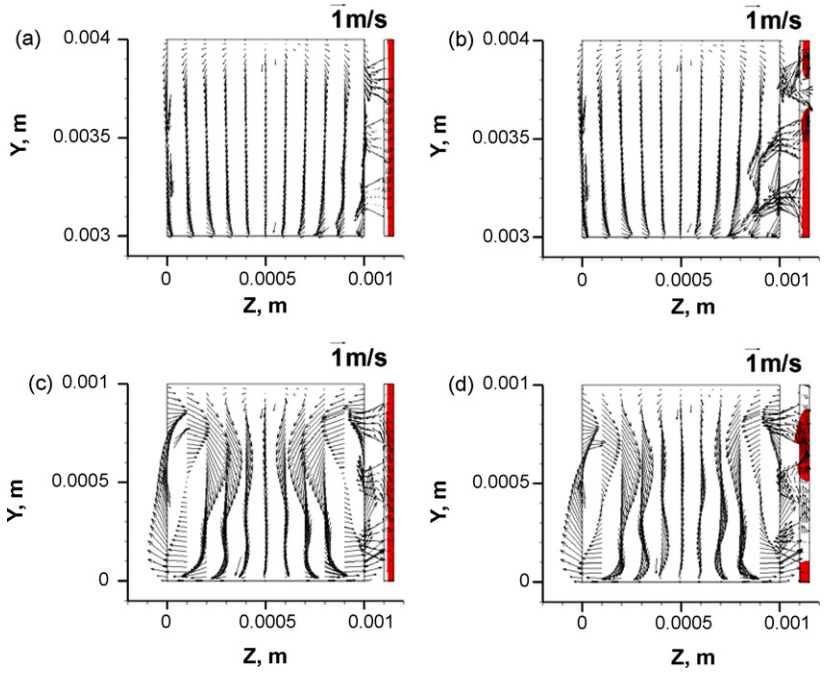

Fig. 25. Water distribution and velocity field on the plane at $x = 0.00205$ m in both inlet and outlet sections for Case 3 ((a) $t = 0.0001$ s at inlet section; (b) $t = 0.0005$ s at inlet section; (c) $t = 0.0001$ s at outlet section; (d) $t = 0.0005$ s at outlet section).

from the porous holes would flow to each other and produce stronger air flow, which could facilitate breaking up the water films.

From Fig. 26, the water film was deformed and then broken up. The small pieces of liquid water suffered air flows from its surrounding holes and they were compressed by those air flows. As those pieces of liquid water were compressed, they would move across the only path, which are the porous holes between the surrounding holes. Therefore, liquid water flowed across these holes into the gas flow channel. However, water was still not fully flowing out of the MEA. The water was not only left around the end walls but also between the porous holes. As discussed in Case 1, the liquid water had difficulties to stay between the porous holes. However, if the balance between the surrounding air flows could be achieved, such conditions would still be possible.

Fig. 27 shows the liquid water distribution and velocity fields on the center plane of the straight section at the inlet. As the water film was broken up, similar to the situation shown in Fig. 26, small pieces of liquid water were formed. The difference in this condition is that the small pieces of liquid water surrounding holes were next to each other without any hole between them. While the liquid water was compressed, it had no path to flow through. In such conditions, two results were observed. One was as shown in Fig. 27a–c while the other is presented in Fig. 27d and e. From Fig. 27a–c, there was a small piece of liquid water on the left hand side between two porous holes. It was compressed and then disappeared. This is because the flow from the liquid water's surrounding holes was not balanced and the liquid water flowed along the strongest air flow to another place. From Fig. 27d and e the balance between those holes was achieved. There was a piece of liquid water between two porous holes which did not move because the forces from the surrounding holes were balanced. From the first three cases, Case 3 had the least amount of water between the holes because the air flow was the strongest in this case.

3.3.2. Water occupation fraction variation

Figs. 28–30 show the water occupation fraction inside the MEA, catalyst layer and GDL, respectively. In contrast to the first two cases, the straight sections achieved better water removal than the corner in both the catalyst layer and the GDL. Even though it has been shown that the secondary flow around the corner was still stronger than at the straight sections, the different kinds of micro-structures of the GDL could still enhance water removal ability significantly resulting in better water drainage at the straight sections than at the corner. Similar water occupation fraction variations were also observed. The straight section at the outlet achieved better water removal than at the inlet, and when the balance was achieved, the variations became almost constant.

3.3.3. Comparison of different micro-structures of GDL

Figs. 31 and 32 show the comparison of the water amount variation inside the MEA and the catalyst layer for the three cases. From the figures, Case 3 showed increased water-removal ability than the other two cases. As mentioned, the only difference between the three cases was the micro-structures of the GDL. Because of its ability to enhance the air flow inside the catalyst layer, the trapeziform porous holes with the minimum area facing the gas flow channel could achieve the best water

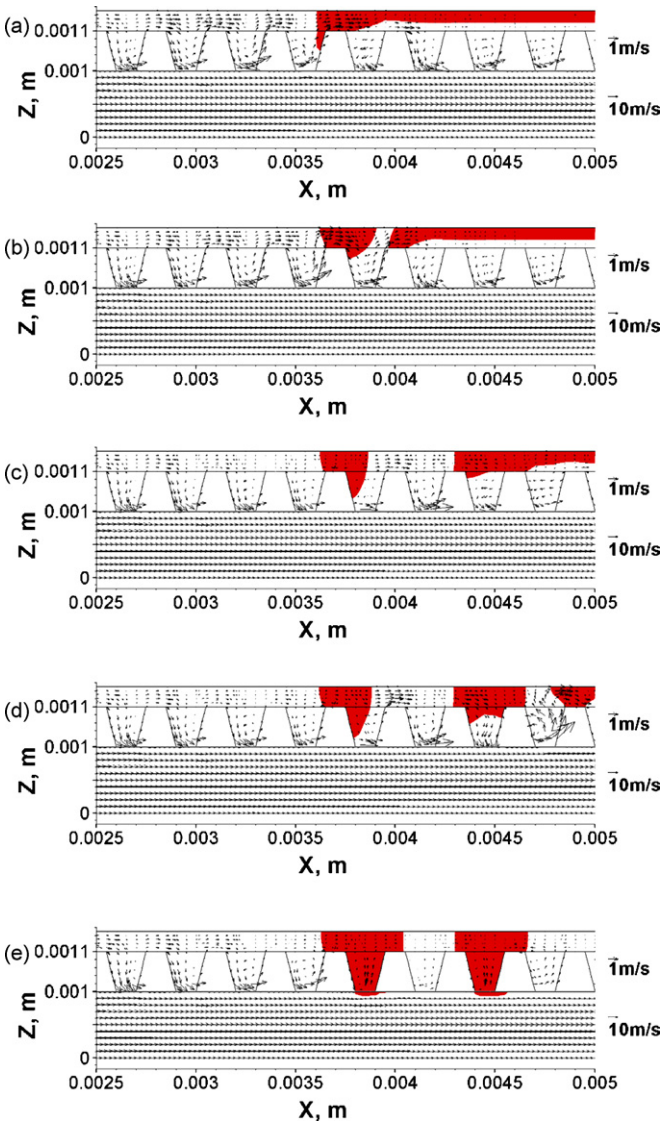

Fig. 26. Water distribution and velocity field on the center-plane ($y = 0.0005$ m) in outlet section for Case 3 (2× magnification along the z-direction for the MEA, 3× minification along the z-direction for the flow channel) ((a) $t = 0.0012$ s; (b) $t = 0.0013$ s; (c) $t = 0.0019$ s; (d) $t = 0.002$ s; (e) $t = 0.003$ s).

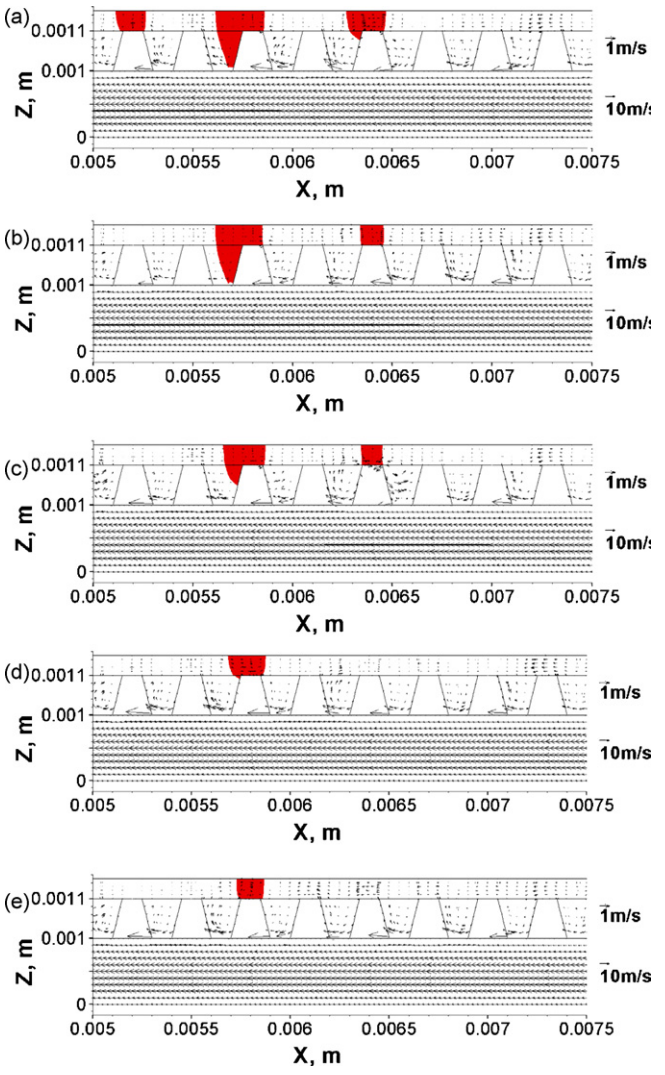

Fig. 27. Water distribution and velocity field on the center-plane ($y = 0.0035$ m) in inlet section for Case 3 (2× magnification along the z-direction for the MEA, 3× minification along the z-direction for the flow channel) ((a) $t = 0.0045$ s; (b) $t = 0.005$ s; (c) $t = 0.006$ s; (d) $t = 0.007$ s; (e) $t = 0.02$ s).

drainage. The worst condition was when the air flow inside the catalyst became weak i.e. when the trapeziform porous holes with the minimum area facing the catalyst layer. Therefore, the key factor to design the GDL is trying to enhance the air flow inside the catalyst layer. Even though Case 3 achieved the best water drainage, the amount of water inside the GDL in Case 3 was the largest, seen from Fig. 33. As discussed above, liquid water was compressed by its surrounding air flows to flow through the porous holes into the gas flow channel. However, the main flow stream inside the gas flow channel was another external force exerted on the liquid water. Therefore, the balance between air and water could be achieved inside the porous holes and thus the water would stay inside the porous holes without going elsewhere as observed in Fig. 26. This could explain why Case 3 had the largest amount of water inside the GDL.

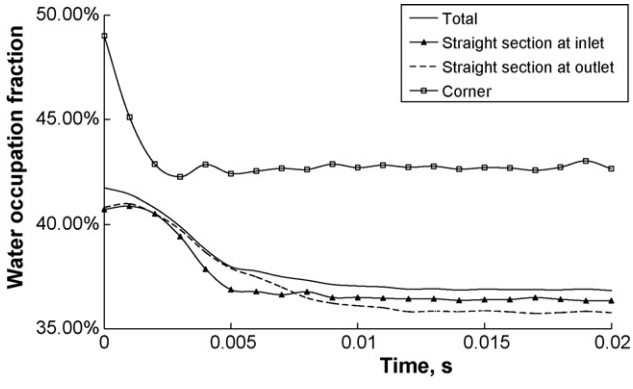

Fig. 28. Water occupation fraction inside the MEA for Case 3.

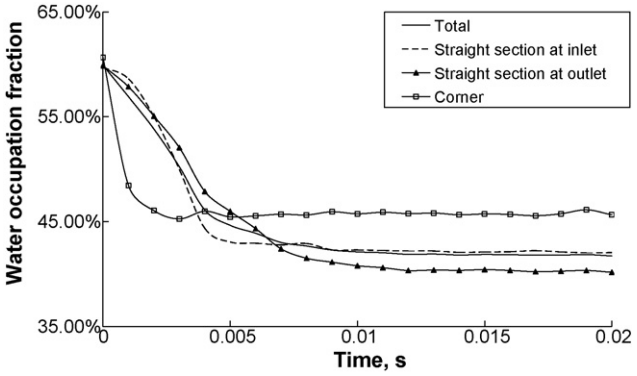

Fig. 29. Water occupation fraction inside the catalyst layer for Case 3.

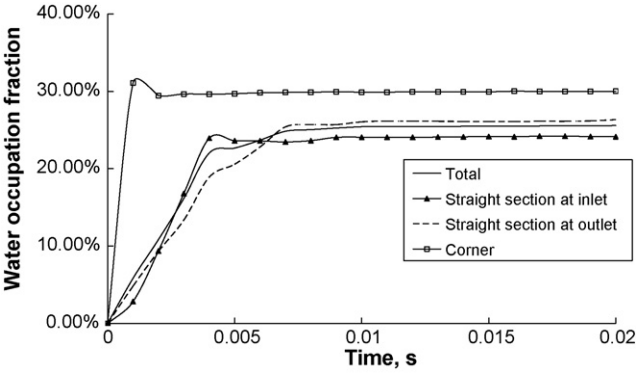

Fig. 30. Water occupation fraction inside the GDL for Case 3.

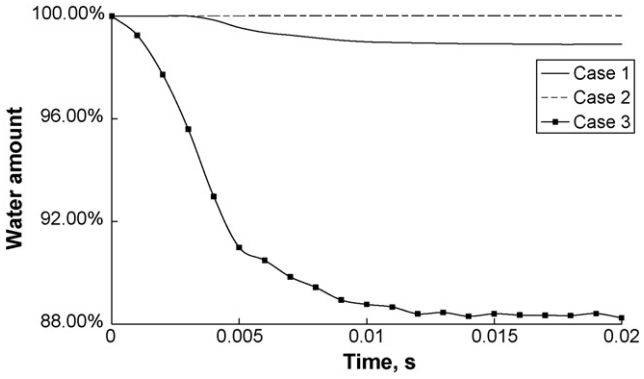

Fig. 31. Water amount variation inside the MEA for the three cases.

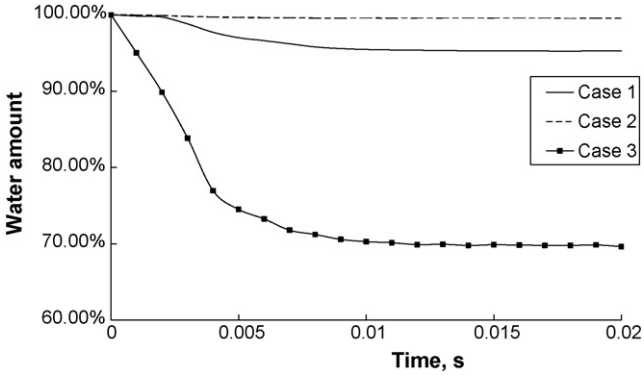

Fig. 32. Water amount variation inside the catalyst layer for the three cases.

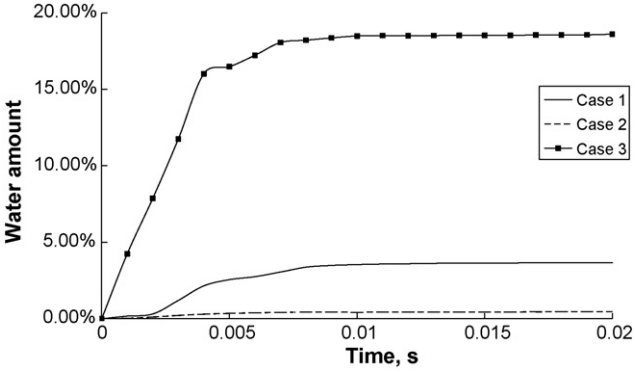

Fig. 33. Water amount variation inside the GDL for the three cases.

4. Conclusions

In this paper, three innovative GDLs with different micro-structures have been proposed and investigated to resolve the challenges existing in conventional GDLs, i.e., the random and arbitrary micro-structure and small pore size do not allow a well-organized liquid water flow across GDL to gas flow channel. The liquid water behaviours in the proposed innovative GDLs together with serpentine gas flow channel on cathode side of a PEM fuel cell were studied by employing a 3D, unsteady, two-phase model in FLUENT with an initial water distribution. By investigating the flow behaviours of liquid water and air-flow velocity fields, the following water management issues have been identified:

1. For serpentine PEM fuel cells, it is easier for the water films to break up at the corner than at the straight sections. This is mainly attributable to the stronger secondary flow at the corner.
2. For the straight sections of the serpentine PEM fuel cells, there is improved water drainage at the downstream of the corner than the upstream. This is mainly attributable to stronger secondary flow at the downstream of the corner.
3. The flow direction inside the catalyst layer is mainly dominated by the water distribution and not the main flow direction inside the gas flow channel.
4. The abruption of liquid water films would start from the initial ruptures and spread to other areas.
5. Residual water inside the catalyst layer is unavoidable. This is because the water stops moving when the balance between all the forces (surface tension, wall adhesion, etc.) is achieved.
6. For the catalyst layer, the areas under the lands of the bipolar plate and the areas close to the surrounding walls are the most possible places that liquid water would stay; other areas suffer from strong air flow and are not surrounded by any walls thus are relatively harder to maintain liquid water.
7. Liquid water inside the catalyst layer will tend to reach a force balance by touching both the top and bottom surfaces. This is the most stable condition for liquid water because

the force due to the wall adhesion effects is the maximum while the effect of the surface tension between air and liquid water is the minimum.

8. Although water was removed faster at the corner, some parts of the water did not flow into the gas flow channel; they flowed into other parts of the MEA, which is still not good for PEM fuel cell performance.
9. The more water removed from the catalyst layer, the more possibility that the GDL contains more water.
10. The general water transport features may not be significantly affected by the micro-structures of the GDL. However, the water removal characteristics and ability could be affected by different shapes of the porous holes of the GDL.
11. For the three innovative micro-structures investigated here, the best water removal is achieved with the trapeziform porous holes with the minimum area facing the gas flow channel due to its ability to enhance the air flow inside the catalyst layer. The worst condition was when the air flow inside the catalyst became the weakest i.e. when the trapeziform porous holes with the minimum area facing the catalyst layer. Therefore, the key factor to design the GDL is trying to enhance the air flow inside the catalyst layer.
12. Even though secondary flow around the corner was still stronger than at the straight sections, the well-designed micro-structures of the GDL could still enhance water removal ability resulting in better water drainage at the straight sections than at the corner.
13. A well-designed GDL can result in better water drainage than conventional GDL.

Some suggestions could be made to manage liquid water in an efficient way as follows:

1. Keeping the maximum area of the porous holes facing the catalyst layer may result in better water drainage, thus the performance could become more stable. On the hand, the minimum area of the porous holes must be avoided to face the catalyst layer.
2. The strong secondary flow at the corner could facilitate water drainage.
3. The good combination of the serpentine flow channels and the well-designed GDLs may result in better water drainage.

Acknowledgements

The authors are grateful for the support of this work by the Auto21^{TM} Networks of Centres of Excellence (Grant D07-DFC), the Natural Sciences and Engineering Research Council of Canada (NSERC), the Canada Foundation for Innovation (CFI), the Ontario Innovation Trust (OIT), and the Graduate School at the University of Windsor.

References

[1] J. Larminie, A. Dicks, Fuel Cell Systems Explained, 2nd ed., John Wiley & Sons, New York, 2000.
[2] J.S. Yi, J.D. Yang, C. King, AIChE J. 50 (2004) 2594.
[3] C.Y. Wang, Chem. Rev. 104 (2004) 4727.
[4] S. Um, C.Y. Wang, K.S. Chen, J. Electrochem. Soc. 147 (2000) 4485.
[5] S. Dutta, S. Shimpalee, J.W. Van Zee, J. Appl. Electrochem. 30 (2000) 135.
[6] E. Hontanon, M.J. Escudero, C. Bautista, P.L. Garcia-Ybarra, L. Daza, J. Power Sources 86 (2000) 363.
[7] S.W. Cha, R. O'Hayre, Y. Saito, F.B. Prinz, J. Power Sources 134 (2004) 57.
[8] A.A. Kulikovsky, Electrochem. Commun. 3 (2001) 460.
[9] Z.H. Wang, C.Y. Wang, K.S. Chen, J. Power Sources 94 (2001) 40.
[10] L. You, H. Liu, Int. J. Heat Mass Transfer 45 (2002) 2277.
[11] U. Pasaogullari, C.Y. Wang, J. Electrochem. Soc. 152 (2005) A380.
[12] H. Meng, C.Y. Wang, J Electrochem. Soc. 152 (2005) A1733.
[13] Y. Wang, C.Y. Wang, J. Electrochem. Soc. 153 (2006) A1193.
[14] H. Meng, C.Y. Wang, Chem. Eng. Sci. 59 (2004) 3331.
[15] H. Ju, C.Y. Wang, J. Electrochem. Soc. 151 (2004) A1954.
[16] H. Ju, C.Y. Wang, S. Cleghorn, U. Beuscher, J. Electrochem. Soc. 153 (2006) A249.
[17] Y. Wang, C.Y. Wang, J. Power Sources 153 (2006) 130.
[18] P. Quan, B. Zhou, A. Sobiesiak, Z. Liu, J. Power Sources 152 (2006) 131.
[19] K. Jiao, B. Zhou, P. Quan, J. Power Sources 154 (2006) 124.
[20] K. Jiao, B. Zhou, P. Quan, J. Power Sources 157 (2006) 226.
[21] X.G. Yang, F.Y. Zhang, A. Lubawy, C.Y. Wang, Electrochem. Solid-State Lett. 7 (2004) A408.
[22] F.Y. Zhang, X.G. Yang, C.Y. Wang, J. Electrochem. Soc. 153 (2006) A225.
[23] J.H. Nam, M. Kaviany, Int. J. Heat Mass Transfer 46 (2003) 4595.
[24] H. Dohle, R. Jung, N. Kimiaie, J. Mergel, M. Muller, J. Power Sources 124 (2003) 371.
[25] U. Pasaogullari, C. Wang, Electrochem. Acta 49 (2004) 4359.
[26] S. Freni, G. Maggio, E. Passalacqua, Mater. Chem. Phys. 48 (1997) 199.
[27] Fluent 6.2 User's Guide, Fluent Inc., 2005.